ARTICLES

Photolysis and Spectroscopy of Vibrationally Excited C−H Overtones of $CHFCl_2$

Aviva Melchior, Xiangling Chen, Ilana Bar,*,† and Salman Rosenwaks

Department of Physics, Ben-Gurion University of the Negev, Beer-Sheva 84105, Israel

Received: March 1, 2000; In Final Form: May 26, 2000

Photodissociation of jet-cooled vibrationally excited $CHFCl_2$ coupled with mass spectroscopic detection of ^{35}Cl ($^2P_{3/2}$) [Cl], ^{35}Cl ($^2P_{1/2}$) [Cl*], ^{37}Cl ($^2P_{3/2}$), ^{37}Cl ($^2P_{1/2}$), and H photofragments was performed. It enabled determination of Cl*/Cl and H/[Cl* + Cl] branching ratios and measurement of the action spectra of the $N = 3$, $N = 7/2$, and $N = 4$ CH stretch−bend polyads. Enhanced C−Cl and C−H bond breaking was observed for all the initially prepared C−H stretch−bend states demonstrating that energy is not preserved in the initial state but rather flows into the other part of the molecule. The yield of Cl* photofragments was found to be about half that of Cl for ∼235 nm photolysis of vibrationally excited $CHFCl_2$. The action spectra are significantly narrower than the room-temperature photoacoustic spectra due to reduction of the rotational inhomogeneous structure. The action spectra also enabled one to resolve the components arising from the different isotopomers of the precursor and a resonance splitting attributed to a local resonance of the $7/2_1$ polyad component with a combination of the $7/2_3$ component and the ClCCl bending. This splitting reflects a ∼3 ps period for the vibrational redistribution and indicates that the coupling of the stretch−bend mixed state to the rest of the molecule is weaker than the stretch−bend coupling itself.

Introduction

Exploration of chemical transformations and of the crucial role played by vibrational energy in processes that involve bond formation or rupture is continuing to intrigue both theoreticians and experimentalists. Deposition of energy in vibrations that are strongly coupled to the reaction coordinate, provided intramolecular vibrational redistribution (IVR) is slow as compared to reaction, may affect photodissociation pathways and control product identity.[1,2] The most evident example of bond selectivity involves the triatomic prototype, i.e., the HOD molecule, for which excitation of fundamental O−H and O−D stretch levels[3] or overtones of O−H[4,5] and O−D[6] affects its photodissociation outcome. Tetraatomic molecules also showed that vibrational excitation influences dramatically photofragment identity and internal state distribution as manifested by HNCO,[7] C_2H_2,[8,9] C_2HD,[10] and H_2O_2 and HOOD.[11,12]

Nevertheless, the field of molecular dynamics evolves toward the study of more complex systems. Therefore, others and ours efforts are directed toward the study of vibrationally mediated photodissociation (VMP) of even larger molecules. Due to the existence of anharmonic resonances and Coriolis interactions and therefore more rapid rates of vibrational energy flow in these molecules, it is anticipated that selective bond rupture will become more difficult. However, vibrational preexcitation might alter the dynamics, particularly when more than one excited potential energy surface (PES) participates. In that case, adiabatic and nonadiabatic interplay may be of importance during photodissociation, as shown by CH_3Cl and CHD_2Cl,[13] CH_3CFCl_2,[14] CF_3I,[15] and the above-mentioned C_2H_2[8,9] and HNCO[7] molecules. Lambert and Dagdigian[13] studied CH_3Cl and CHD_2Cl excited to the fourth C−H stretch overtone. They found that the yield of atomic Cl from the VMP of CH_3Cl is higher, meaning that couplings mix the C−H stretch motion to C−Cl dissociation coordinate more effectively in CH_3Cl than in CHD_2-Cl. Also, they attributed a slight preferential formation of D over H in ∼243 nm VMP of CHD_2Cl ($\nu_{CH} = 5$) to the more efficient coupling of the C−H stretch to the C−D stretches rather than to the bends as in CH_3Cl. In addition, they showed that the above vibrational excitation changes the branching ratio between the spin−orbit states Cl ($^2P_{1/2}$) [Cl*] and Cl ($^2P_{3/2}$) [Cl] products in 235 and 238 nm photodissociation. Very recently, we showed that photodissociation of preexcited fundamental symmetric CH_3 stretch (ν_{CH}), and the second ($3\nu_{CH}$) and third ($4\nu_{CH}$) overtones of CH_3CFCl_2,[14] increased the yield of all three photofragments (Cl, Cl*, and H) and affected the branching into Cl and Cl*. This demonstrated that the energy was intramolecularly coupled from the excited methyl C−H bond into the C−Cl stretch that became the major cleaved bond and that the preexcitation affected dynamics as seen from the altered Cl*/Cl ratio. Also, Butler and co-workers[15] showed that variation of the temperature of the CF_3I molecules in a supersonic expansion, which influences the initial vibrational state, alters the relative yields of electronically excited and ground-state iodine obtained in photodissociation.

In addition, VMP serves as a means for acquisition of action spectra and hence less congested vibrational spectra, owing to the use of cooled samples in supersonic expansions. The VMP action spectroscopy benefits from the signal enhancement provided by a better Franck−Condon (FC) overlap of the

† Present address: The Institute for Chemistry & Chemical Technology, The Institutes for Applied Research, Ben-Gurion University of the Negev, Beer-Sheva 84105, Israel.

10.1021/jp000791r CCC: $19.00
Published on Web 08/08/2000

initially prepared state with the upper PES. It affords sensitivities that are high enough to detect vibrational excitation of molecules at the low density of the supersonic expansion. Usually, these spectra sustain determination of molecular constants and identification of different isotopomers, specific couplings, and more accurate primary time scales for energy redistribution.[7,9,14,16,17] In favorable cases they allow to resolve additional bands and to determine the splittings that lead to secondary time scales for redistribution. Determination of these splittings, which correspond to longer time scales, carry valuable information on the pathways of vibrational coupling in vibrationally excited molecules and may provide a clearer picture of the dominant couplings.

This paper reports the room-temperature photoacoustic (PA) and the jet-cooled action spectra of the $N = 3$, $N = 7/2$, and $N = 4$ CH stretch−bend polyad components (see below) of dichlorofluoromethane, $CHFCl_2$ (HCFC-21), and the photodissociation of these states by ∼235/243 nm photons. Dubal and Quack[18] studied the room-temperature vibrational spectra of $CHFCl_2$ up to 12 000 cm^{-1}, and Moore and co-workers[19] extended it up to 16 500 cm^{-1}. The observed spectra were interpreted quantitatively in terms of a multiple anharmonic resonance interactions for stretching and bending motions of the C−H chromophore. We obtained the above-mentioned polyad components by direct IR excitation and subsequent excitation by ∼235/243 nm photons. The UV excitation promoted the molecule to the upper PESs, where it decomposed and released Cl, Cl*, and H photofragments, allowing monitoring of action spectra. Due to the coupling between the prepared C−H states and the C−Cl bond, the later was effectively broken. The action spectra reveal details of the vibrational dynamics that occur after the C−H stretch excitation and allow resolving the dominant isotopomers.

Experimental Section

The experimental setup consisted of two tunable lasers and a home-built Wiley−McLaren time-of-flight mass spectrometer (TOFMS)[14,20] which allowed sensitive and mass-selective detection. One laser operated in the near-IR and induced the vibrational excitation of the $CHFCl_2$ molecules, and the second, in the UV, photodissociating and subsequently probing the photofragments by (2 + 1) resonantly enhanced multiphoton ionization (REMPI).

The vibrational overtone excitation pulses in the region between 875 and 1180 nm came from an idler beam of an optical parametric oscillator (bandwidth ∼0.08 cm^{-1}) pumped by the third harmonics output of a Nd:YAG laser. The beam was focused with a 30 cm focal length (f.l.) lens onto the interaction region of the TOFMS. The counterpropagating photolysis/probe UV laser beam at ∼235/243 nm was obtained from the doubled output of a tunable dye laser (bandwidth ∼0.5 cm^{-1}) pumped by the third harmonics of another Nd:YAG. It was delayed by 15 ns and focused onto the ionization region with a 30 cm f.l. lens. Special care was taken to bring the two beams collinearly to a common focus in the center of the ionization region of the TOFMS. Typical energies of ∼5, ∼7, and ∼7 mJ for the excitation of the $N = 3$, $N = 7/2$, and $N = 4$ CH stretch−bend polyad components, respectively, and ∼120 μJ for the UV were employed. Only when the overtone excitation was induced the UV laser photolyzed the $CHFCl_2$ molecules effectively. This is due to a very low absorption cross section (∼10^{-23} cm^2) at the wavelengths employed for photodissociation (∼240 nm).[21] When the $CHFCl_2$ was preexcited, the photodissociation was considerably enhanced with respect to the 235 nm photodissociation, due to a favorable FC factor.

The laser beams (∼6 ns pulses) entered the chamber perpendicularly to both the TOFMS axis and the molecular beam axis. $CHFCl_2$ (Aldrich, 98%) prepared as a 10% mixture in Ar, at a total pressure of 760 Torr, expanded through a 0.8 mm orifice of a pulsed valve (PV) and a 2 cm long tube of 0.9 mm diameter connected to it. The molecular beam traveled another ∼2 cm to the chamber center where it was intersected by the lasers. Two turbomolecular pumps evacuated both the source chamber and the ion detector chamber, respectively. The base pressure in both chambers was 2×10^{-8} Torr, and when the PV was on (driven with a voltage pulse of 120 V, ∼190 μs, 10 Hz), the pressure increased to 1.2×10^{-5} Torr. It is assumed that these expansion conditions result in a predominant rotational temperature of ∼15 K and vibrational temperature of < 100 K. This relies on the VMP of the second C−H stretch overtone of propyne, seeded in Ar under similar conditions, where the rotationally resolved action spectra were simulated with the above temperatures.[22] The rotational and vibrational temperatures inferred for $CHFCl_2$ are roughly similar to that of propyne.

The photofragments were detected by two-photon transitions, corresponding to H ($2s\ ^2S \leftarrow 1s\ ^2S$) at 243.135 nm,[23] Cl ($4p\ ^2D_{3/2} \leftarrow 3p\ ^2P_{3/2}$) at 235.336 nm, and Cl* ($4p\ ^2P_{1/2} \leftarrow 3p\ ^2P_{1/2}$) at 235.205 nm.[24] Ions formed via REMPI in the focal volume were subjected to continuously biased extraction, two acceleration stages, a field-free drift region and finally detection by a microsphere plate. The detector output was amplified and fed into a digital oscilloscope. Wavelength-dependent mass spectra of ^{35}Cl, $^{35}Cl^*$, ^{37}Cl, $^{37}Cl^*$, and H photofragment ion peaks were processed with a boxcar integrator and a computer. The ^{37}Cl and $^{37}Cl^*$ photofragments were monitored simultaneously with ^{35}Cl and $^{35}Cl^*$, respectively, using an additional boxcar channel and taking advantage of the TOFMS mass resolution. Scanning the IR beam wavelength resulted in jet-cooled action spectra of the different photofragments. Each data point in the ensuing spectra was an average of 30 pulses.

The Cl*/Cl and H/[$^{35}Cl + {}^{35}Cl^* + {}^{37}Cl + {}^{37}Cl^*$], denoted as H/[Cl + Cl*], branching ratios were determined by fixing the IR wavelength on the Q-branch of the corresponding polyad components. The UV laser was scanned to get Doppler profiles of the tagged photofragments or fixed on the wavelength of maximum signal to obtain the amplitude of the corresponding photofragment. The Doppler profiles of the photofragments could be well fitted by Gaussian functions. The widths of the Cl and Cl* photofragments were similar, governed by the laser width, while that of H was ∼5.5 times larger, exhibiting the higher translational energy acquired by the H photofragment. The ratios could be obtained from the peak area ratios and thus from the measured amplitudes and profile widths. The amplitudes were obtained by measuring the signal resulting from VMP (for ∼2000 pulses) and then by blocking the excitation beam and monitoring the very small background due to the UV one photon photodissociation. This background was subtracted to obtain the net VMP signal. The procedure was repeated, and the branching was obtained as an average of 8−10 sets. In addition to the measured amplitudes and profile widths the intensity factors for the employed transitions were taken into account. To correct the experimental REMPI intensities of the above-mentioned transitions of Cl* and Cl a scaling factor was employed, as obtained from the recent measurement of Ashfold and co-workers.[25] The H/[Cl + Cl*] ratios were obtained by taking into account the H to ^{35}Cl relative intensity factor, as calculated from the known REMPI signal ratio of the 193 nm photodissociation of HCl,[23] the ^{37}Cl isotope abundance, and the measured Cl*/Cl branching ratio.[26]

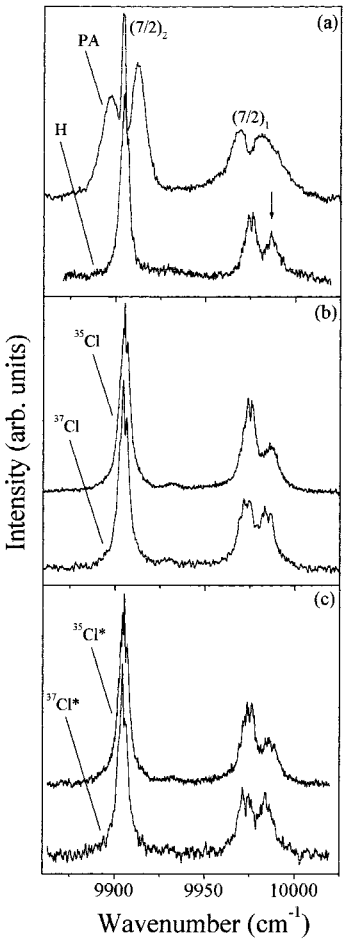

Figure 1. Vibrational overtone excitation spectra of the dominant features of the $N = 7/2$ polyad of $CHFCl_2$: (a) photoacoustic absorption spectrum and H action spectrum; (b) ^{35}Cl and ^{37}Cl action spectra; (c) $^{35}Cl^*$ and $^{37}Cl^*$ action spectra. The arrow designates the $7/2_3 + \nu_6$ combination band observed only in the action spectra due to congestion elimination. The intensity scale is different for each trace.

PA spectroscopy detected the acoustic signal produced by vibrational excitation at room temperature by converting the vibrational energy absorbed in the sample to translational energy. Introducing a window into the excitation beam path and diverting a small portion of it toward an auxiliary PA cell allowed simultaneous measurement of the PA signal. The split beam was focused, with a 10 cm f.l. lens, near a microphone. Pressure of 300 Torr of $CHFCl_2$ in the PA cell enabled monitoring of the PA signal when the IR frequency matched the transition. The PA signal was fed into an amplifier and then into an additional boxcar channel.

For wavelength calibration, rovibrational overtone transitions of water were monitored by PA spectroscopy in the wavelength regions corresponding to the $N = 3$ and $N = 4$ CH stretch−bend polyad components of $CHFCl_2$. The positions of the water absorption lines were compared to the HITRAN database[27] and calibrated accordingly and so were the spectral features of $CHFCl_2$.

Results and Discussion

a. PA and Action Spectra. The room-temperature PA spectra along with the jet-cooled action spectra in the regions of the $7/2_1$, $7/2_2$ and 4_1, polyad components are shown in Figures 1 and 2, respectively. The PA spectra were assigned by employing the model suggested by Dubal and Quack[18] that involves

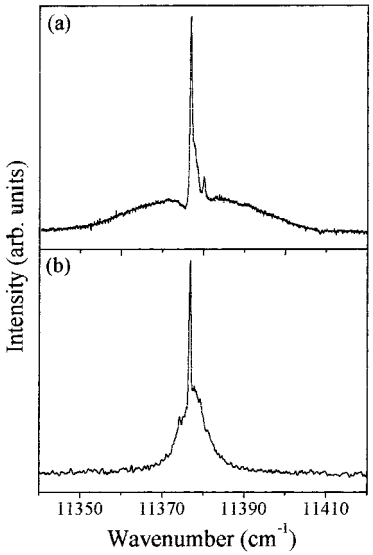

Figure 2. Vibrational overtone excitation spectra of the 4_1 polyad component of $CHFCl_2$: (a) Photoacoustic absorption spectrum; (b) H action spectrum. The intensity scale is different for each spectrum.

coupling between the CH stretching and the CH bending motions. The vibrational overtone bands were labeled as N_j components, using their nomenclature. An integral N represents the polyad quantum number that consists of N CH stretch quanta in the zero-order bright state, while a half-integral N contains N CH stretch quanta combined with the higher ($\nu_2 = 1317.2$ cm^{-1}) or lower frequency bending ($\nu_7 = 1242.6$ cm^{-1}). In this model the CH stretch ($\nu_1 = 3024.8$ cm^{-1}) is anharmonically coupled by the 1:2 Fermi resonance with either of the two CH bends and the two bends are coupled by a Darling−Dennison resonance. These resonances lead to a mixing of states that form the polyad components. These components were labeled by j, starting from the highest frequency to the lowest.

The PA spectrum of the $N = 7/2$ polyad was found to be similar to the Fourier transform IR (FTIR) spectrum of Dubal and Quack.[18] A portion of it is presented in the upper trace (a) of Figure 1 and it includes the main features observed for this polyad. Several additional peaks of much lower intensity were observed at lower frequencies, and they also corresponded to those observed in the FTIR spectrum. The appearance of only two prominent peaks in the $N = 7/2$ polyad and of one in the $N = 3$ and $N = 4$ is due to the low CH bend frequencies which interact relatively weakly via the Fermi resonance with the CH stretch. It is worth noting that, in CHF_2Cl, where the Fermi resonance is closer in energy, more bands of comparable intensity were observed in each polyad.[19]

The bands observed in the PA spectra are of different types, and they represent the contributions resulting from three dominant isotopomers $[CHF^{35}Cl_2]$:$[CHF^{35}Cl^{37}Cl]$:$[CHF^{37}Cl_2] \cong$ 9:6:1 according to the occurrence of the two stable Cl isotopes. These bands are related approximately to CH stretch overtones and to their combinations with bends and therefore possess different shapes, depending on the character of the involved vibrations. The $CHFCl_2$ is an asymmetric top ($\kappa = -0.59$)[28] that belongs to the C_s point group for identical chlorine atoms and is reduced to C_1 for different chlorine isotopes. In the former, the ν_1 CH stretch and the ν_2 CH bend are of a′ and the ν_7 CH bend of a″ symmetry, while in the latter the CH stretch and bends are of type a.[29,30] From the rotational constants of the isotopomers with identical chlorine atoms (C_s),[28,30] the A bands (a″) are predicted to have a sharp medium Q branch with well-defined P and R envelopes, while the B and C bands (a′)

should exhibit hybrid contours with dominant character of either B or C.[31] Indeed, the 3_1 and 4_1 components demonstrate C type prevalancy, the $7/2_1$ B type and the $7/2_2$ which is a combination of the stretch with the bend of a″ is of A type.

The observed PA spectra represent not only contributions from the dominant isotopomers of $CHFCl_2$ but also contain transitions that are related to the hot bands observed in the fundamental region.[29,30] The $CHFCl_2$ comprises several fundamentals of low frequency < 1000 cm^{-1}, the lowest being the ClCCl bending, ν_6 (a′) at 277.2 cm^{-1}. Therefore, ~37% of the population are in these low vibrations at room temperature (compared to the zero point level population of 63%). It is expected that they will appear in the proximity of the C−H polyad components but at lower frequency (due to often negative values of the anharmonicity constants).

Comparison of the PA spectrum with the action spectra of the H, ^{35}Cl, ^{37}Cl, $^{35}Cl^*$, and $^{37}Cl^*$ photofragments (Figure 1, lower trace of panel a and panels b and c) of the $7/2_1$, $7/2_2$ polyad components show the extensive contraction that occurs in the latter, due to the rotational cooling. Similar behavior was observed for the 3_1 polyad component and also for the 4_1 component (Figure 2). This narrowing and the merging of the P and R branches with the Q branch result in an almost undistinguishable PQR envelopes in A and C bands and in a much narrower B band. The polyad components in the jet-cooled action spectra exhibit overall contours in the range 19−25 cm^{-1} in comparison to 45−60 cm^{-1} for the room temperature spectra. This clearly indicates that most of the spectral widths in the room-temperature spectra arise from rotational inhomogeneous broadening.

At first glance, the action spectra corresponding to the different photofragments seem to be similar; however, careful comparison shows that they differ somewhat. This is since each of the photofragments represents photodissociation of different isotopomers. The H action spectra are a result of the photodissociation and the release of the H atoms by all three $CHFCl_2$ isotopomers, while the ^{35}Cl or $^{35}Cl^*$ are derived from $CHF^{35}Cl_2$ and $CHF^{35}Cl^{37}Cl$ and ^{37}Cl or $^{37}Cl^*$ from $CHF^{35}Cl^{37}Cl$ and $CHF^{37}Cl_2$. In fact, the signal obtained by subtraction of the action spectra of ^{37}Cl from that of ^{35}Cl (both were measured simultaneously) provides spectra that cancel the contribution from the mixed isotopomer $CHF^{35}Cl^{37}Cl$ and are mainly related to the spectra of $CHF^{35}Cl_2$ (~90% $CHF^{35}Cl_2$−10% $CHF^{37}Cl_2$). On the other hand, the ^{37}Cl spectra correspond mainly to the mixed isotopomer (76%) and to the $CHF^{37}Cl_2$ (24%). Since the contribution of the corresponding isotopomers dominates, it is anticipated that by locating the peaks of the Q branches or the center of the B type band of the subtracted spectra and of the ^{37}Cl, the positions of the $CHF^{35}Cl_2$ and the isotopomeric shifts related to $CHF^{35}Cl^{37}Cl$ can be obtained. The Q-branch maxima and band center for the $CHF^{35}Cl_2$ isotopomers are 8708 ± 1, 9975 ± 1, 9905.5 ± 1, and 11 387 ± 1 cm^{-1} and the shifts are 0.4 ± 0.1, 2.0 ± 0.1, 0.9 ± 0.3, and 0.23 ± 0.01 cm^{-1} for the 3_1, $7/2_1$, $7/2_2$, and 4_1 polyad components, respectively. A similar approach, where isotopically selected $^{35,37}Cl$ atomic photofragments were detected, was employed by Hippler and Quack.[16] This allowed identification of the bands resulting from the different isotopomers in the region of the third C−H overtone transition of $CHCl_3$.

An important advantage provided by action spectra is the congestion reduction, which allows in favorable cases observation of new features that are otherwise overlaid by other bands. An example of a new feature that is not observed in the PA spectrum is shown in the action spectra of the $7/2_1$ region. The

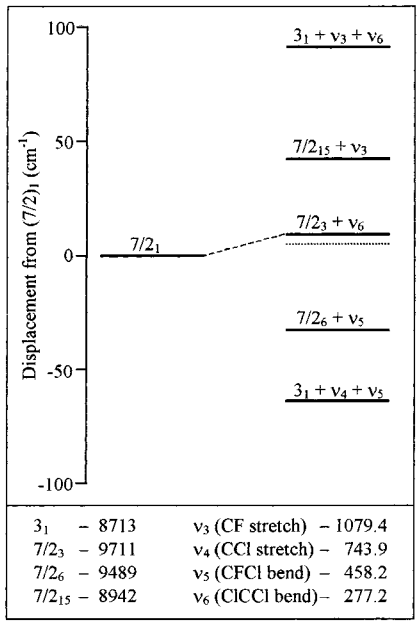

Figure 3. Schematic representation of the calculated states of a′ symmetry in the vicinity of the $7/2_1$ component. The dotted line indicates the position of the deperturbed state. The lower panel includes the frequencies (cm^{-1}) of the presented polyad components as calculated from the model of Dubal and Quack[18] and of the fundamental modes.[29,30]

separation between the $7/2_1$ component and the new feature, indicated by the arrow (Figure 1), is 13 ± 1 cm^{-1}, and the ratio of their integrated intensities is 0.7 to 0.3, respectively. Employing the simple two-level model[31] to describe the resonance and using the observed energies of the perturbed bands and the relative intensities, the unperturbed energies (the diagonal elements) which are coupled by the off-diagonal coupling constant, *W*, can be determined. Using energies of 9988 and 9975 cm^{-1} for the perturbed bands of the $CHFCl_2$ isotopomer and their relative intensities of 0.3 and 0.7, respectively, enables derivation of the zero-order energies 9984 and 9979 cm^{-1} and $|W| = 6$ cm^{-1}.

The importance of low-order resonances, which involve the change of three or four vibrational quanta and can be coupled via third- and fourth-order anharmonic terms in the vibrational Hamiltonian, in controlling vibrational energy redistribution was shown for several molecules.[32,7d,16b,17b,e] Therefore, it is anticipated that this type of coupling could be involved here as well. An energy level diagram of possible perturbing states of a′ symmetry that could be coupled via cubic or quartic terms to the $7/2_1$ state of similar symmetry, within ±100 cm^{-1} is displayed in Figure 3. The energies of the possible perturbing states were obtained by calculating the values of the involved polyad components (based on the model of Dubal and Quack[18]) and considering the energies of the other fundamental modes.[29,30] It is expected that these energies are somewhat higher than the energies of the perturbing states since the off-diagonal anharmonicities that are usually small and negative were not accounted for. As seen from Figure 3, almost all states are quite separated from the $7/2_1$ state, except the $7/2_3 + \nu_6$ state which involves a higher polyad component, $7/2_3$, and the ν_6 ClCCl bend. It is likely that this is the only state that could be coupled by *W* of ~6 cm^{-1}, which was found above. The energy of the $7/2_3 + \nu_6$ state that amounts to 9988 cm^{-1} is in close agreement with the zero-order energy of 9983.8 cm^{-1} of the feature mentioned above (dotted line in Figure 3), and the small energy mismatch should not be prohibitive when the anharmonicities

are included. The combination of the $7/2_3$ component with the ClCCl mode seems very likely since they are very close in energy, as demanded by the deperturbation.

Moreover, this resonance is expected to be observed in the range of $7/2_1$ component, due to the energy proximity. However, it is less likely that it will appear in the range of the $5/2_1$ and $9/2_1$ polyad components. Again, calculating the positions of the $5/2_3$ and $9/2_3$ components together with the contributions of the ClCCl bending locates the $5/2_3 + \nu_6$ at 7146 cm^{-1} and the $9/2_3 + \nu_6$ at 12 715 cm^{-1}. These states are much too far separated from $5/2_1$ at 7205 cm^{-1} and $9/2_1$ at 12 636 cm^{-1} for the observation of the weak coupling. Indeed, monitoring of the action spectra in the region of the $N = 9/2$ polyad revealed no additional features, except the $9/2_1$ and $9/2_2$ components. This shows that the perturbing state is tuning into resonance when going from the $5/2_1$ region to the $7/2_1$ region and then detunes in the $9/2_1$ region.

The splitting between the $7/2_1$ component and the nearly resonant state indicates that the period of the vibrational oscillation is of $1/c\Delta\nu$, or ∼3 ps, and the redistribution time is of ∼1.5 ps to the ClCCl bend. This is ∼30 times longer than the time of redistribution between stretch and bend, i.e., 50 fs, which was deduced by us in the computation of the time evolution from the effective Hamiltonian.[18] The longer time is a measure of the time scale for energy flow between the $7/2_1$ and $7/2_3 + \nu_6$ zero-order states, when the former is prepared. A similar behavior was observed in some other molecules with isolated C−H stretches. Hippler and Quack[16b] found that in $CHCl_3$ the energy redistribution from the 4_1 state to the CCl_3 "umbrella" vibration is almost a factor of 100 slower than the ∼50 fs redistribution time between stretch and bend. The latter time in CHF_3 is also similar[33,34] and is faster than the oscillation of the vibrational energy between the 5_3 state and a dark state that occurs with a typical time scale of ∼4−5 ps. Also, in the homologous CH_3CFCl_2[14b] the splittings between the CH_3 stretch−deformation states of the second and third overtone manifolds correspond to redistribution time of 0.3−0.7 ps. This is somewhat faster than the vibrational redistribution between the highest frequency component of the $4\nu_{CH}$ and a dark state in its vicinity that occurs on a 0.9 ps time scale.

b. Branching Ratios. The action spectra (Figures 1 and 2) do not only provide a wealth of dynamical information concerning the prepared vibrational states but also exhibit and emphasize the significant increase in yield of Cl, Cl*, and H photoproducts as a result of VMP, relative to the background one photon photodissociation. Therefore, by measurement of the yields of the different photofragments and particularly the branching ratios between them, some information concerning the dynamics on the upper PESs can be revealed. Since different products are released in the VMP process it is essential to ensure that their formation is under similar conditions enabling quantitative evaluation of the yields provided by the specific photodissociating channels. Therefore, ln−ln plots of the H, ^{35}Cl, and $^{35}Cl^*$ REMPI ion signals against the UV laser energy were carried out to find the UV energetic region that shows a linear dependence. All these plots resulted in slopes close to three. As mentioned above, the UV laser serves for both photodissociation and REMPI detection of the photofragments. The observed cubic dependence for the H, Cl, and Cl* photoproducts was attributed to one-photon photolysis and to REMPI detection via two-photon excitation, followed by a saturated ionization step. Employing UV laser energy in the above-mentioned range and keeping similar energies and focusing conditions for the IR and UV lasers enabled measurement and comparison of the REMPI signals of the different photofragments. The REMPI signals obtained in the VMP depend on the vibrational excitation efficacy, the absorption from the prepared vibrational state to the upper PESs, and the branching into the particular channel. The enhancement in photodissociation was deduced by normalizing the REMPI signal to the PA signal, which reflects the efficacy of the vibrational excitation, and to the background signal resulting from photodissociation of vibrationless ground-state $CHFCl_2$. These results show that the total Cl yield, in both spin−orbit states, was enhanced four times more than H for the VMP of the 3_1, $7/2_2$, and 4_1 components. It shows that although the C−H stretch is initially extended, the cleavage of the C−Cl bond is more efficient. This is in line with the analysis in the previous section that showed that the vibrational energy redistribution occurs on a time scale of picoseconds. Therefore, for the pulse widths employed in our experiment it is obvious that mixed states were prepared and the energy was already redistributed into the modes corresponding to the heavy atoms during the excitation step. Extension of the C−Cl bond, which becomes the reaction coordinate, probably leads to a favorable FC factor with the upper PESs. This might be due to the absorption characteristics related to a $\sigma^*_{C-Cl} \leftarrow$ n transition.[35,36]

TABLE 1: Cl*/Cl and H/[Cl + Cl*] Branching Ratios in Vibrationally Mediated Photodissociation of $CHFCl_2$

	3_1	$7/2_2$	4_1
energy[a] (cm^{-1})	51 200	52 397	53 869
Cl*/Cl	0.52 ± 0.13	0.48 ± 0.09	0.49 ± 0.10
H/[Cl + Cl*][b]	0.15 ± 0.08	0.14 ± 0.08	0.11 ± 0.06

[a] The energy represents the combined energy used in VMP of $CHFCl_2$ when Cl was tagged. [b] The combined energy for H is 1363 cm^{-1} lower than for Cl, which might affect the determined H/[Cl + Cl*] ratios.

By accounting for the transition probability ratios of the tagged fragments,[23,25,26] one can convert REMPI signals into Cl*/Cl and H/[Cl + Cl*] branching ratios. The branching ratios are listed in Table 1 together with the combined energies for Cl tagging. It is seen that the Cl*/Cl in VMP of $CHFCl_2$ is close to 0.5 independent of the prepared polyad component. The H/[Cl + Cl*] is in the range of 0.11−0.15 showing that H production occurs to some extent, but its fraction is quite low compared to the Cl and Cl*. It is worth noting that the combined energy (IR + UV) for photodissociation of $CHFCl_2$ differs somewhat for H and Cl due to the use of the same UV laser for photodissociation and probing. For H atom tagging the combined energy is 1363 cm^{-1} lower than for Cl which might affect somewhat the H/[Cl + Cl*] ratio. However, this difference is < 3% from the total combined energy of ∼52 000 cm^{-1}.

The VMP Cl*/Cl branching ratios are comparable to the ratio of 0.54 ± 0.12 obtained in the ∼235 nm photodissociation of $CHFCl_2$, although the total photodissociation energy in the latter is significantly lower. Also, similar ratios were obtained in the VMP of $3\nu_{CH}$ and $4\nu_{CH}$ of CH_3CFCl_2,[14] showing preference of Cl over Cl*. Due to the lack of dynamical calculations, which aid the interpretation of the spin−orbit branching ratios, the determination of the involved states and couplings is difficult. Nevertheless, Huber and co-workers[37] found for 193 nm photodissociation of $CHFCl_2$ an anisotropy parameter β of 0.5. This was attributed to a partial loss of anisotropy arising from a geometrical rearrangement during dissociation or from a small contribution of an electronic transition of $A' \leftarrow A'$ symmetry overlapping the dominant $A'' \leftarrow A'$ transition. The $A'' \leftarrow A'$ transition moment is perpendicular to the CHF molecular plane and parallel to the line connecting the two Cl atoms.

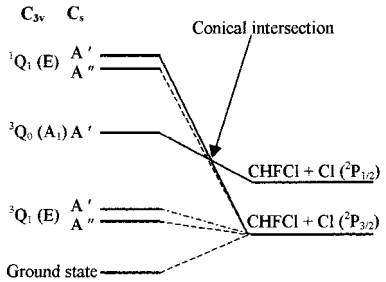

Figure 4. Correlation diagram for $CHFCl_2$ photodissociation.

Some idea about the involved states can be obtained from studies on the related molecules CH_3Cl and CH_3I. Lambert and Dagdigian[13] found in the case of one-photon photolysis and VMP of CH_3Cl that only the $^3Q_0$ state is initially accessed, similar to CH_3I. In CH_3I the first absorption band comprises three dipole-allowed states, $^1Q_1$, $^3Q_0$, and $^3Q_1$, corresponding to the 3E, $2A_1$, and 2E states in C_{3v} symmetry.[39−43] The parallel $^3Q_0$ transition correlates with $CH_3 + I^*$, while the other two perpendicular transitions correlate with $CH_3 + I$. The occurrence of I products with similar anisotropy to that of I* was attributed to nonadiabatic transition between the $^3Q_0$ and the $^1Q_1$. As seen from Figure 4, in C_s symmetry the $^3Q_0$ transforms to an A′, while the E states split into A′ and A″ components. The A′ states can couple via the radial derivative term in the Hamiltonian.[15,39] Similar states are presumed for $CHFCl_2$ as well, although the split between the Cl spin−orbit states is much smaller than in I probably leading to determination of Cl*/Cl at large CHFCl−Cl separation as calculated for the analogous HCl.[44] Assuming similar accessibility of the upper electronic states as in the 193 nm photodissociation of $CHFCl_2$, predominant absorption to an A″ state that correlates with Cl is expected in the VMP as well. However, direct absorption to the A′ state that is connected to Cl* or to the A′ state that correlates with it via nonadiabatic transitions must occur to account for the significant production of Cl*. Nevertheless, the possibility of different accessibility of the involved PESs cannot be ruled out. Further experiments that measure the anisotropy parameter in VMP are necessary to resolve this definitively.

Conclusions

The vibrational overtone spectra provided by the VMP of $CHFCl_2$ display the polyad components and show the enhancement in photodissociation as a result of vibrational excitation. The vibrational spectra of the cold molecules reveal C−H polyad components that are significantly narrower than the room-temperature PA spectra due to the reduction in inhomogeneous broadening. The narrowing together with the isotopically selected $^{35,37}Cl$ atomic photofragments detection allowed identification of the bands resulting from the dominant isotopomers of $CHFCl_2$. In addition it afforded observation of a new feature in the region of the $7/2_1$ component that was attributed to a resonance with a near lying state that represents a combination between $7/2_3$ and the ClCCl bend. The splitting between these states corresponds to a redistribution time of ∼1.5 ps to the ClCCl bend compared to the ∼30 times faster redistribution between C−H stretch and bend. The energy flow from the initially excited C−H to the C−Cl bond is also evident from the enhancement of the Cl and Cl* photofragments that results from favorable FC overlap with the upper PESs. The combination of action spectroscopy with branching ratios determination sheds light on the dynamics of the vibrationally excited states and the upper PESs.

Acknowledgment. We thank Professor P. J. Dagdigian for useful discussions. This research was supported by Grant No. 96-00140 from the United States-Israel Binational Foundation (BSF), by Grant No. I0537098.05/97 from the German-Israel Binational Foundation (GIF), and by the James Franck Binational German-Israeli Program in Laser-Matter Interaction. A.M. thanks the Israeli Ministry of Science for a Levy Eshkol scholarship.

References and Notes

(1) Nesbitt, D. J.; Field, R. W. *J. Phys. Chem.* **1996**, *100*, 12735.
(2) Crim, F. F. *J. Phys. Chem.* **1996**, *100*, 12725.
(3) Bar, I.; Cohen, Y.; David, D.; Arusi-Parpar, T.; Rosenwaks, S.; Valentini, J. J. *J. Chem. Phys.* **1991**, *95*, 3341. Bar, I.; Cohen, Y.; David, D.; Rosenwaks, S.; Valentini, J. J. *J. Chem. Phys.* **1990**, *93*, 2146.
(4) Vander Wal, R. L.; Scott, J. L.; Crim, F. F.; Weide, K.; Schinke, R. *J. Chem. Phys.* **1991**, *94*, 3548. Vander Wal, R. L.; Scott, J. L.; Crim, F. F. *J. Chem. Phys.* **1990**, *92*, 803.
(5) Brouard M.; Langford, S. R. *J. Chem. Phys.* **1997**, *106*, 6354.
(6) Cohen, Y.; Bar, I.; Rosenwaks, S. *J. Chem. Phys.* **1995**, *102*, 3612.
(7) (a) Brown, S. S.; Metz, R. B.; Berghout, H. L.; Crim, F. F. *J. Chem. Phys.* **1996**, *105*, 6293. (b) Brown, S. S.; Berghout, H. L.; Crim, F. F. *J. Chem. Phys.* **1995**, *102*, 8440. (c) Berghout, H. L.; Brown, S. S.; Delgado, R.; Crim, F. F. *J. Chem. Phys.* **1998**, *109*, 2257. (d) Coffey, M. J.; Berghout, H. L.; Woods, E., III; Crim. F. F. *J. Chem. Phys.* **1999**, *110*, 10850.
(8) Zhang, J.; Riehn, C. W.; Dulligan, M.; Wittig, C. *J. Chem. Phys.* **1995**, *103*, 6815.
(9) Schmid, R. P.; Ganot, Y.; Bar, I. Rosenwaks, S. *J. Chem. Phys.* **1998**, *109*, 8959. Schmid, R. P.; Arusi-Parpar, T.; Li, R.-J.; Bar, I.; Rosenwaks, S. *J. Chem. Phys.* **1997**, *107*, 385. Arusi-Parpar, T.; Schmid, R. P.; Ganot, Y.; Bar, I.; Rosenwaks, S. *Chem. Phys. Lett.* **1998**, *287*, 347.
(10) Schmid, R. P.; Ganot, Y.; Bar, I. Rosenwaks, *J. Mol. Struct.* **1999**, *480−481*, 197. Arusi-Parpar, T.; Schmid, R. P.; Li, R.-J.; Bar, I.; Rosenwaks, S. *Chem. Phys. Lett.* **1997**, *268*, 163.
(11) Brouard, M.; Martinez, M. T.; O'Mahony, J.; Simons, J. P. *J. Chem. Soc., Faraday Trans.* **1989**, *285*, 1207.
(12) Brouard, M.; Martinez, M. T.; O'Mahony, J.; Simons, J. P. *Mol. Phys.* **1990**, *69*, 65.
(13) (a) Lambert, H. M.; Dagdigian, P. J. *J. Chem. Phys.* **1998**, *109*, 7810. (b) Lambert, H. M.; Dagdigian, P. J. *Chem. Phys. Lett.* **1997**, *275*, 499. (c) Melchior, A.; Lambert, H. M,; Dagdigian, P. J.; Bar, I.; Rosenwaks, S. *Isr. J. Chem.* **1997**, *37*, 455.
(14) (a) Melchior, A.; Chen, X.; Bar, I.; Rosenwaks, S. *Chem. Phys. Lett.* **1999**, *315*, 421. (b) Melchior, A.; Chen, X.; Bar, I.; Rosenwaks, S. *J. Chem. Phys.* **2000**, *112*, 10787.
(15) Person, M. D.; Kash, P. W.; Butler, L. J. *J. Chem. Phys.* **1991**, *94*, 2557.
(16) (a) Hippler, M.; Quack, M. *Ber. Bunsen-Ges. Phys. Chem.* **1997**, *101*, 356. (b) Hippler, M.; Quack, M. *J. Chem. Phys.* **1996**, *104*, 7426. (c) Hippler, M.; Quack, M. *Chem. Phys. Lett.* **1994**, *231*, 75.
(17) (a) Boyarkin O. V.; Rizzo, T. R. *J. Chem. Phys.* **1996**, *105*, 6285. (b) Boyarkin, O. V.; Settle, R. D. F.; Rizzo, T. R. *Ber. Bunsen-Ges. Phys. Chem.* **1995**, *99*, 504. (c) Boyarkin, O. V.; Rizzo, T. R.; Perry, D. S. *J. Chem. Phys.* **1999**, *110*, 11359. (d) Boyarkin, O. V.; Rizzo, T. R.; Perry, D. S. *J. Chem. Phys.* **1999**, *110*, 11346. (e) Boyarkin, O. V.; Lubich, L.; Settle, R. D. F.; Perry, D. S.; Rizzo, T. R. *J. Chem. Phys.* **1997**, *107*, 8409.
(18) Dubal, H.-R.; Quack, M. *Mol. Phys.* **1984**, *53*, 257.
(19) Wong, J. S.; Green, W. H., Jr.; Cheng, C. K.; Moore, C. B. *J. Chem. Phys.* **1987**, *86*, 5994.
(20) Wiley, W. C.; McLaren, I. H. *Rev. Sci. Instrum.* **1955**, *26*, 1150.
(21) Hubrich, C.; Zetzsch C.; Stuhl, F. *Ber. Bunsen. Ges. Phys. Chem.* **1977**, *81*, 437.
(22) Ganot, Y.; Chen, X.; Bar, I.; Rosenwaks, S. Unpublished data.
(23) Matsumi, Y.; Tonokura, K.; Kawasaki, M.; Tsuji, K.; Obi, K. *J. Chem. Phys.* **1993**, *98*, 8330.
(24) Liyanage, R.; Yang, Y.; Hashimoto, S.; Gordon, R. J.; Field, R. W. *J. Chem. Phys.* **1995**, *103*, 6811.
(25) Regan, P. M.; Langford, S. R.; Ascenzi, D.; Cook, P. A.; Orr-Ewing, A. J.; Ashfold, M. N. R. *Phys. Chem. Chem. Phys.* **1999**, *1*, 3247.
(26) Melchior, A.; Knupfer, P.; Bar, I.; Rosenwaks, S.; Laurent, T.; Volpp, H.-R.; Wolfrum, J. *J. Phys. Chem.* **1996**, *100*, 13375.
(27) Rothman, L. S.; Rinsland, C. P.; Goldman, A.; Massie, S. T.; Edwards, D. P.; Flaud, J.-M.; Perrin, A.; Camy-Peyret, C.; Dana, V.; Mandin, J.-Y.; Scroeder, J.; McCann, A.; Gamache, R. R.; Wattson, R. B.; Yoshino, K.; Chance, K.; Jucks, K.; Brown, L. R.; Nemtchinov, V.; Varanasi, P. *The 1996 HITRAN Molecular Spectroscopic Database and HAWKS (HITRAN Atmospheric Workstation)*; Atomic and Molecular Physics Division, Harvard-Smithsonian Center for Astrophysics.
(28) McLay, D. B. *Can. J. Phys.* **1964**, *42*, 720.

(29) Baldacci, A.; Passerini A.; Ghersetti, S. *Spectrochim. Acta* **1984**, *40A*, 165.

(30) Snels, M.; Quack, M. *J. Chem. Phys*. **1991**, *95*, 6355.

(31) Herzberg, G. *Molecular Spectra and Molecular Structure. II Infrared and Raman Spectra of Polyatomic Molecules*; Van Nostrand Reinhold Co.: New York, 1945.

(32) Stuchebrukhov, A. S.; Marcus, R. A. *J. Chem. Phys*. **1993**, *98*, 6044.

(33) Segall, J.; Zare, R. N.; Dubal, H. R.; Lewerenz, M.; Quack, M. *J. Chem. Phys*. **1987**, *86*, 634.

(34) Dubal, H. R.; Quack, M. *J. Chem. Phys*. **1984**, *81*, 3779.

(35) Robin, M. B. *Can. J. Chem*. **1985**, *63*, 2032.

(36) Okabe, H. *Photodissociation of Small Molecules*; John Wiley & Sons: New York, 1978.

(37) Yang, X.; Felder, P.; Huber, J. R. *Chem. Phys*. **1994**, *189*, 124.

(38) Melchior, A.; Bar, I.; Rosenwaks, S. *J. Chem. Phys*. **1997**, *107*, 8476.

(39) Yabushita, S.; Morokuma, K. *Chem. Phys. Lett*. **1988**, *153*, 517.

(40) Amatatsu, Y.; Morokuma, K.; Yabushita, S. *J. Chem. Phys*. **1991**, *94*, 4858.

(41) Amatatsu, Y.; Yabushita, S.; Morokuma, K. *J. Chem. Phys*. **1996**, *104*, 9783.

(42) Guo, H.; Schatz, G. C. *J. Chem. Phys*. **1990**, *93*, 393.

(43) Guo, H.; Lao, K. Q.; Schatz, G. C.; Hammerich, A. D. *J. Chem. Phys*. **1991**, *94*, 6562.

(44) Alexander, M. H.; Pouilly, B.; Duhoo, T. *J. Chem. Phys*. **1993**, *99*, 1752. Lambert, H. M.; Dagdigian, P. J.; Alexander, M. H. *J. Chem. Phys*. **1998**, *108*, 4460.